Journal of
Ceramic Science
and Technology

J. Ceram. Sci. Tech., 07 [04] 447-454 (2016)
DOI: 10.4416/JCST2016-00076
available online at: http://www.ceramic-science.com

Influence of $MgAl_2O_4$ Spinel Addition on Properties of Alumina-Chrome Refractory Prepared with Alumina-Chrome Slag

J. Wu, J. Liu, R. Li, Q. Zhen*

Research Center of Nano Science and Technology, Shanghai University, Shanghai 200444, China
received September 27, 2016; received in revised form October 31, 2016; accepted November 26, 2016

Abstract

Alumina-chrome refractory was developed using alumina-chrome slag of different grades (5 ~ 3 mm, 3 ~ 1 mm, 1 ~ 0 mm, 0.088 mm and 0.045 mm), with added micron-grade $MgAl_2O_4$ spinel powders. Batch materials were milled, pressed and sintered at 1500 °C with 22 h soaking. The refractory with 5 wt% $MgAl_2O_4$ exhibited the best properties in terms of bulk density and apparent porosity. In all the refractory samples, new phases were formed as a result of slag-refractory and copper-refractory interaction. With the addition of $MgAl_2O_4$ spinel, the corrosion resistance of the alumina-chrome refractory was improved remarkably.

Keywords: Alumina-chrome refractory, alumina-chrome slag, $MgAl_2O_4$ spinel, slag corrosion, crude copper corrosion

I. Introduction

Alumina-chrome refractory (ACR) can form a substitutional solid solution at high temperature without formation of any eutectic [1]. ACR exhibits effective resistance to chemical corrosion at high temperature, superior mechanical properties and good thermal shock resistance. It has been widely applied in numerous fields, such as carbon black reactors, fiber glass furnaces, metallurgy furnaces and so on [2–8]. Bonar *et al.* [9] reported that ACRs were superior to alumina and magnesia-chrome refractories (MCRs) when exposed to acidic slags. However, the use of ACR in furnaces in the copper industry has not been widely reported. At present, magnesia-chrome type refractories are the most commonly used materials in furnaces in the copper industry. MCRs are alkaline refractories that demonstrate high resistance against alkaline slags generated in the process of copper smelting [10–12]. However, the poor thermal shock resistance of MgO-based materials make it difficult to use in the combustion chamber, since the temperature in the chamber may change drastically and suddenly [13]. Additionally, MCRs are more likely to hydrate during storage. Furthermore, copper-making factories prefer to choose alternative lower-price refractories to reduce the cost. Therefore, a low-cost refractory was required to substitute MCRs.

In this paper, alumina-chrome slag (ACS), a by-product from Cr metal refining based on the thermit process, which contains Al_2O_3 and Cr_2O_3 as its main components, was studied as a raw material for low-cost ACR. ACR is more easily corroded by alkaline slags compared to MCR because Al_2O_3 is an amphoteric oxide. To increase the slag resistance, different amounts of $MgAl_2O_4$ spinel were added. Fe^{3+} and Fe^{2+} from the slag can be trapped in the spinel lattice, thus increasing the slag's viscosity and preventing further permeation [14]. In addition, $MgAl_2O_4$ spinel has the merits of a high melting point and good thermal shock performance.

In this study, chromium corundum magnesium aluminate spinel refractory was synthesized with ACS and spinel powder, and its anti-slag performance was explored in the crucible experiment (1450 °C, 4 h). We adopted X-ray diffraction (XRD), X-ray fluorescence spectrometry (XRF), scanning electron microscopy (SEM) and energy dispersive spectrometry (EDS) to study the effects of the addition of $MgAl_2O_4$ spinel powder on the physicochemical properties and anti-slag and blister copper corrosion properties of the refractory.

II. Experimental Procedure

(1) Raw materials used

ACS with different particle grades (5 ~ 3 mm, 3 ~ 1 mm, 1 ~ 0 mm, 0.088 mm, 0.045 mm), bought from Jinzhou Jixin Industrial co. LTD., was used as the raw material. Al_2O_3-rich $MgAl_2O_4$ spinel powders (0.045 mm) were added. The chemical compositions of these materials were analyzed by means of X-ray fluorescence and are listed in Table 1.

The refractoriness of the ACS was 1780 °C, which suggested that ACR prepared with ACS could easily withstand the temperature in copper industry furnaces (< 1400 °C). The XRD patterns were measured to examine the phase of ACS and Al_2O_3-rich spinel powders, as shown in Fig. 1. These showed that ACS contained chrome corundum, aluminum oxide and calcium aluminate, the Al_2O_3-rich spinel contained spinel and aluminum oxide as its main crystalline phase.

* Corresponding author: qzhen@staff.shu.edu.cn

Table1: The chemical composition the raw materials.

Raw materials	Chemical compositions (wt%)							
	Al_2O_3	Cr_2O_3	MgO	Na_2O	CaO	Fe_2O_3	SiO_2	others
Alumina chrome slag	78.30	14.96	0.57	3.43	1.29	1.19	0.17	0.09
Spinel powder	81.06	-	17.95	-	-	-	-	0.99

Table 2: Ingredients of chromium corundum-spinel refractories.

Number	Aluminum chromium slag mass fraction (wt%)					Spinel powders
	5~3mm	3~1mm	1~0 mm	0.088mm	0.045mm	mass fraction (wt%)
G0	34	28	8	22	8	-
G4	34	28	8	22	4	4
G5	34	28	8	22	3	5
G6	34	28	8	22	2	6
G7	34	28	8	22	1	7

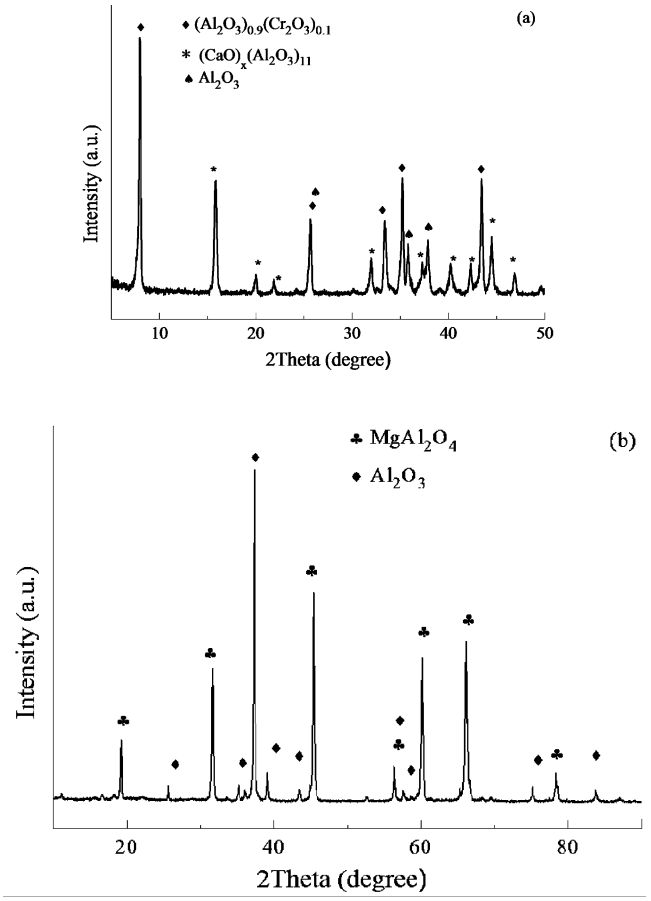

Fig. 1 : The XRD patterns of alumina chrome slag (a) and spinel powder (b).

(2) Material preparation and characterization

The different grades of ACS were uniformly mixed according to the mass ratio of 34 g, 28 g, 8 g and 22 g in total weight of a 100 g sample. 2 wt% phosphoric acid was added, then this raw material was aged for one week (A). Al_2O_3-rich $MgAl_2O_4$ spinel powders (B) were mixed with ACS (0.045 mm) in different ratios. Then raw material B was added to A, and mixed well with aluminum dihydrogen phosphate and polyvinyl alcohol as additives. Afterwards, green cylinders (d = 30 mm, h = 20 mm) were pressed in a steel mold under an axial pressure of 60 MPa. After being dried at 60 °C for 24 h, these cylinders were sintered at 1500 °C for 22 h with a heating rate of 5 °C/min in air. The ingredients of the ACR samples with different additions of $MgAl_2O_4$ spinel powders are listed in Table 2. Bulk density and apparent porosity of the samples were measured according to the Archimedes principle, using water as the immersion liquid.

The refractoriness of ACS was measured according to ISO 528:1983, MOD (NHD refractoriness test furnace). Phase analysis of the raw materials and sintered samples was performed by means of X-ray diffraction (Joel D/max 2000) using CuKα radiation. Chemical compositions of the raw materials were detected using X-ray fluorescence (Shimadu 1800). The microstructure of dense refractory after corrosion was examined using a scanning electron microscope (SU-1500) with an energy-dispersive scanning (wscalab) attachment for qualitative and quantitative micro analysis.

(3) Static slag/copper corrosion experiment on sintered samples

Inner holes with size of F 14 × 12 mm were drilled into the sintered samples to make crucibles. 3.5 g slag (for the slag corrosion) and 3.43 g crude Cu with 1.51 g slag (for the copper corrosion) were placed into the crucibles, respectively. Subsequently, the crucibles were fired at 1450 °C for 4 h in a high-temperature furnace under air atmosphere, and they were then cut along center line after natural cooling. In order to figure out the slag corrosion performance of ACR, the penetration depth at the bottom of a crucible made of re-bonded MCR was also tested as reference. The chemical composition of the slag is shown in Table 3.

Table 3: Chemical composition of the slag.

Chemical composition	SiO_2	Fe_2O_3	CaO	MgO	Al_2O_3	S	Cu
Mass fraction (wt%)	28	60	1	1	5	2	3

III. Results and Discussion

(1) Characterization of sintered refractory

Fig. 2 shows the bulk density and apparent porosity of ACR varied with Al_2O_3-rich spinel content before and after sintering at 1500 °C. It can be observed that the bulk density decreased with the addition of spinel as the lower-density material caused the decrease in the density values (Fig. 2(a)) [15]. Meanwhile, the difference in thermal expansion coefficients between alumina and spinel could lead to microcracks in the matrix during sintering, ultimately increasing the apparent porosity [16]. So it could be seen that after sintering at 1500 °C for 22 h, the bulk density of the ACR firstly increased with increasing amount of spinel and then decreased, the apparent porosity decreased and then increased correspondingly. The samples with 5 wt% Al_2O_3-rich spinel exhibited the highest bulk density of 3.25 g·cm^{-3} and the lowest apparent porosity of 13 %.

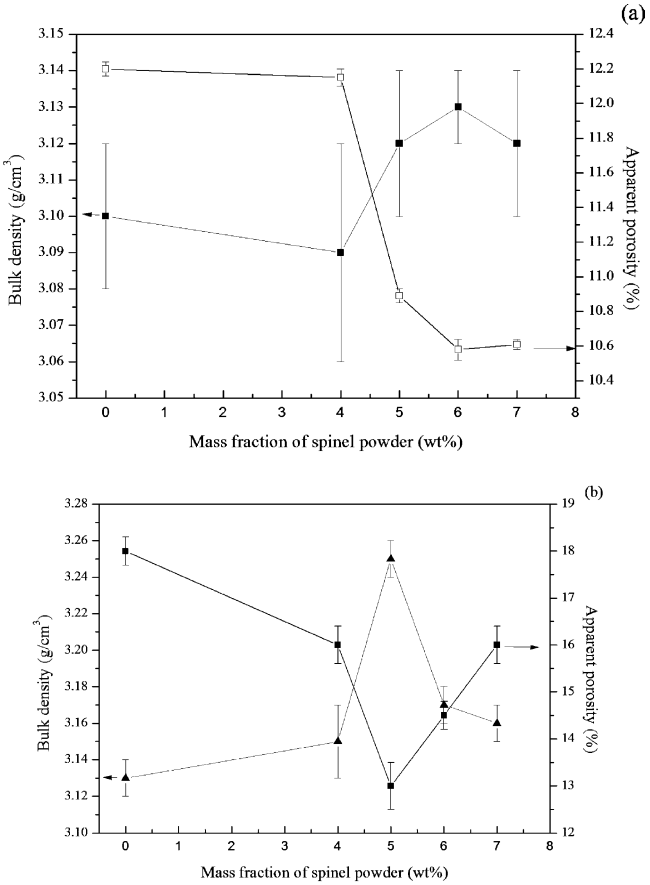

Fig. 2: The bulk density and apparent porosity of products varied with the addition of spinel powders before (a) and after (b) sintering at 1500 °C for 22 h.

The XRD patterns of samples G0 and G5 are shown in Fig. 3. It can be seen that the main phases in sample G0 were chrome corundum and calcium aluminate, agreeing with the phases observed in the ACS. In sample G5, besides chrome corundum and calcium alumina phase, magnesium alumina spinel phase could be observed owing to the addition of spinel powder. It indicated that both phases of G0 and G5 remained stable before and after sintering, no new phase was generated.

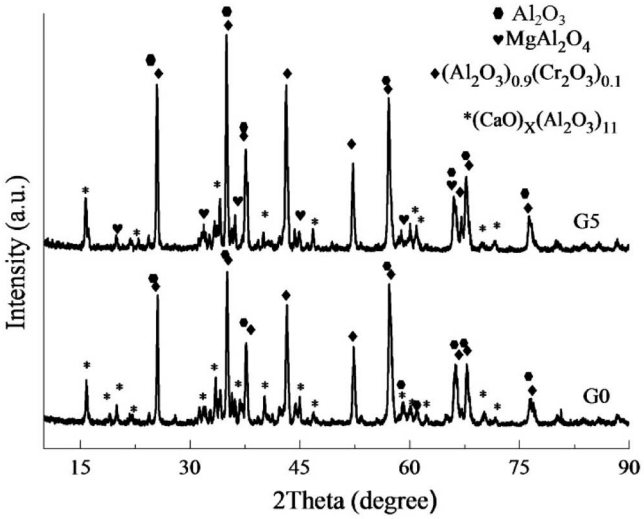

Fig. 3: XRD pattern of aluminum chrome refractory G5 and G0.

(2) Slag/copper metal corrosion behavior of sintered refractory

The photographs of the crucible section morphology after corrosion using slag or copper metal at 1450 °C for 4 h in an air atmosphere are shown in Fig. 4. Details of the slag composition are mentioned in Table 3. It can be seen from the photographs that sample G5 was less corroded by the slag or copper metal than sample G0, because more slag or copper metal was residual. Fig. 4(a) shows that for G0 the corrosion reaction at the three-phase border between the matrix, slag and air was very severe.

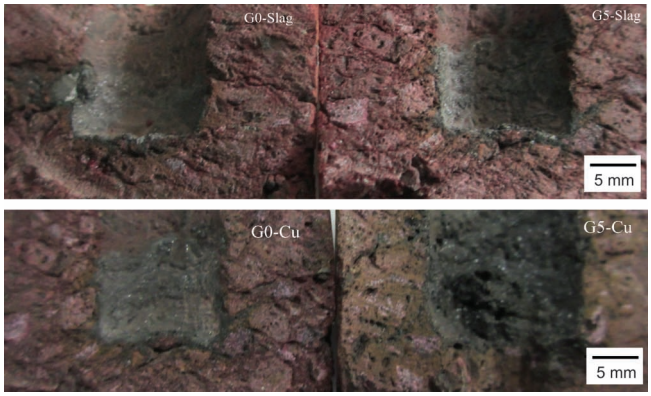

Fig. 4: Digital images of crucible samples after slag/Cu corrosion testing at 1450 °C for 4 h.

Slag corrosion values of ACR with different amounts of Al_2O_3-rich spinel obtained after slag/copper corrosion experiments are shown in Fig. 5(a) and (b), respectively. The slag/copper penetration depths at the bottom of all

the crucibles were measured with digital photos on the scale of 12:1, the corrosion areas were calculated using the box counting method. As can be seen from these figures, when 5 wt% alumina-rich spinel was added to the ACR, the resistance to slag/copper corrosion and penetration were improved significantly. The average penetration depth at the bottom of the crucibles of re-bonded MCR was 2.09 mm, it was about the same as that of the ACR with 5 wt% addition of $MgAl_2O_4$ spinel powder, so it was confirmed that the corrosion resistance of ACR could be improved remarkably after suitable addition of $MgAl_2O_4$ spinel. Compared to the ACR without added spinel, the slag corrosion resistance over the bottom (over the depth of the hole) was improved by 33.3 %. While the copper corrosion resistance over the bottom (over the depth of the hole) was improved by 42.8 %. It has been reported that slag corrosion and penetration resistance was improved after spinel addition to high-alumina bricks [14], a comparable phenomenon was also observed in the ACR in this work.

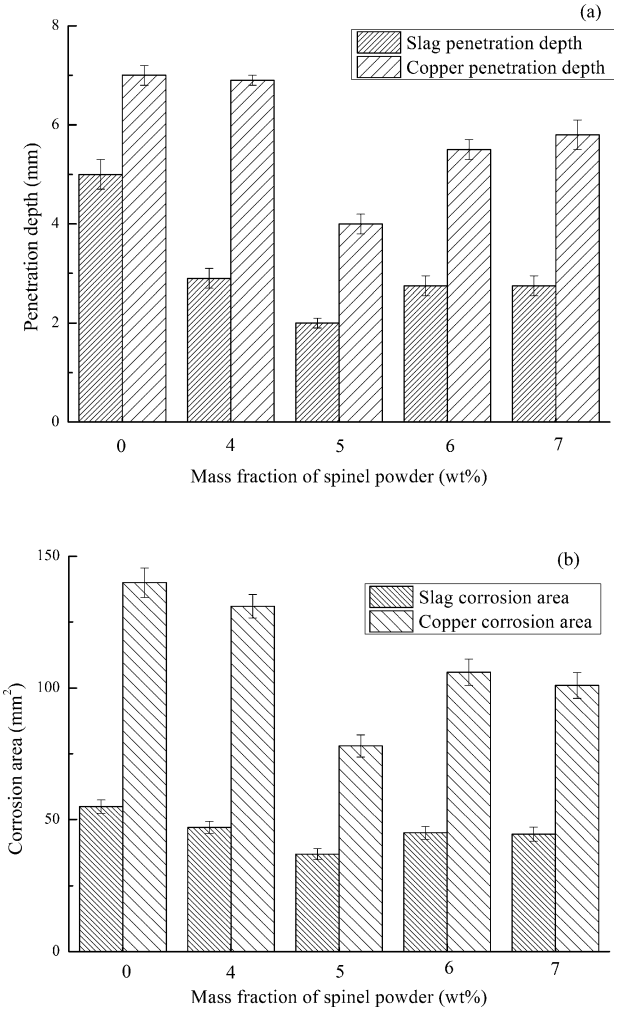

Fig. 5: Slag/copper penetration depth (a) of corrosion area (b) alumina chrome with different spinel amounts tested at 1450 °C for 4 h.

(3) Phases of the crucible samples after corrosion by slag/Cu at 1450 °C

Each sample used for XRD analysis was cut into small sheets and polished to remove any slag remaining on the surface. The XRD patterns of the G0 and G5 refractory after slag corrosion at 1450 °C for 4 h are provided in Fig. 6(a). Besides chrome corundum (main phases in the refractory), iron silicon oxide, $FeCr_2O_4$, was also observed after slag corrosion. Iron silicon oxide was formed by the reaction of FeO and SiO_2, and penetrated into the refractory matrix, while $FeCr_2O_4$ was formed owing to the reaction of the penetrated FeO with chromium corundum in the refractory matrix. And penetrated SiO_2 also reacted with calcium aluminum, forming calcium aluminum silicate. However, in refractory G5, typical peaks of $Mg(Fe, Al)O_4$ were also observed, indicating that FeO from the slag was dissolved into the added spinel crystalline. In fact, part of Al^{3+} in magnesium aluminate spinel was replaced by Fe^{3+} in slag at high temperature. The formation of $Mg(Fe, Al)O_4$ could promote the slag viscosity.

The main phases in the crucible samples after Cu corrosion (Fig. 6(b)) were chrome corundum, $FeAl_2O_4$ and Cu_2O. Cu liquid was oxidized to Cu_2O at 1250 °C as reported in the literature [17]. In the crude copper corrosion process, FeO in the slag reacted with Al_2O_3 and formed $FeAl_2O_4$ with high melting point [8], which could prevent the penetration of Cu liquid through open porosity.

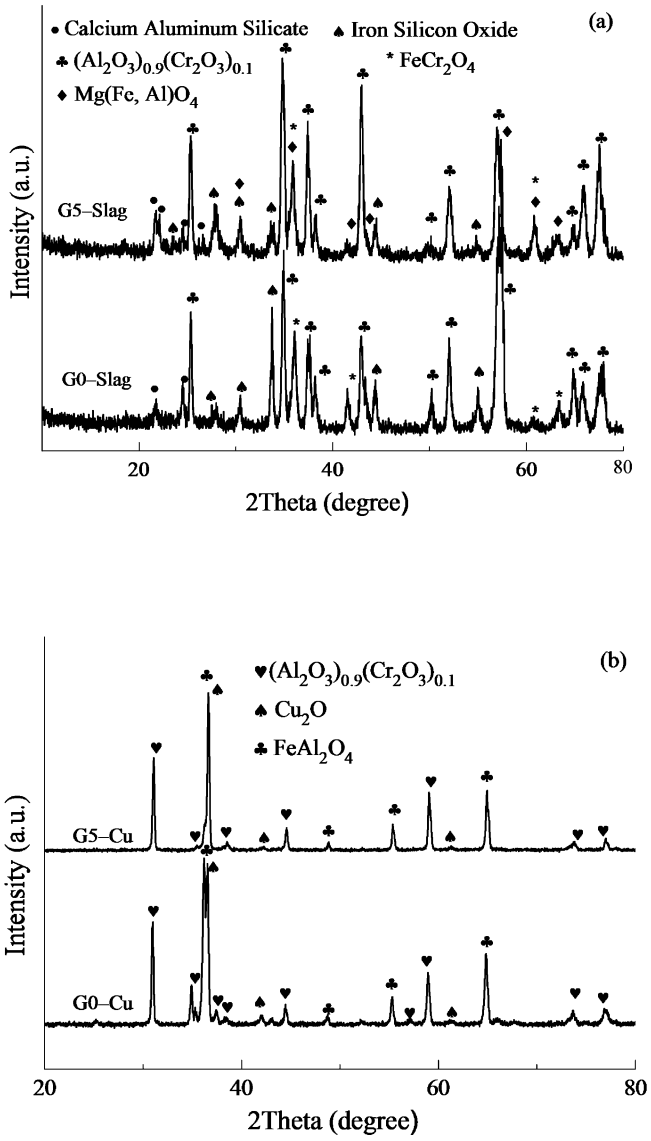

Fig. 6: The interface XRD patterns of G0 and G5 after slag (a)/copper (b) corrosion.

(4) Microstructure changes in the ACR crucible after slag corrosion

The microstructures and the compositions at the conversion zone between the slag and bottom of the ACR crucible after slag corrosion are shown in Fig. 7 and Table 4, respectively. It can be seen that each of the samples had a slag layer on the surface of the matrix, the combination between the matrix and aggregate was extremely tight, which was clearly observed with 100-fold magnification.

The representative micrographs of the interface in samples G0, G5 and G7 after slag corrosion are shown in Fig. 7 (a), (d), (g), respectively. The slag layer and the refractory were observed in each of samples with a clear interface. It could also be observed that the interface of G0 was coarser than that of G5 and G7, which indicated that more serious slag corrosion occurred between the slag and matrix at 1450 °C. Fig. 7 also shows the Fe ((b), (e) and (h)), Si ((c), (f) and (i)) area scanning of the slag-matrix interface analyzed by EDS. Area scanning maps showed the distribution of the main elements in the slag and their respective migration at high temperature. It was also observed that the migration of Fe and Si from the slag to the refractory decreased gradually from the slag-matrix interface to the matrix part, both Fe and Si elements had wider distribution in G0, clear differences between Fe and Si element distribution in the slag and matrix in G5 could be found, suggesting that the penetration speed of melt slag at the high temperature of G5 was slower than in the case of the other samples. The relative contents of Fe_2O_3 and SiO_2 at different points in the slag (1), interface (2) and refractory (3) are given in Table 4. It can be seen that the contents of Fe and Si elements at each point of G5 were lower than in other samples, especially the content of Si. From all the discussions above, the anti-slag penetration performance of G5 proved better than that of the other samples and the mechanism of the anti-slag performance was analyzed as follow.

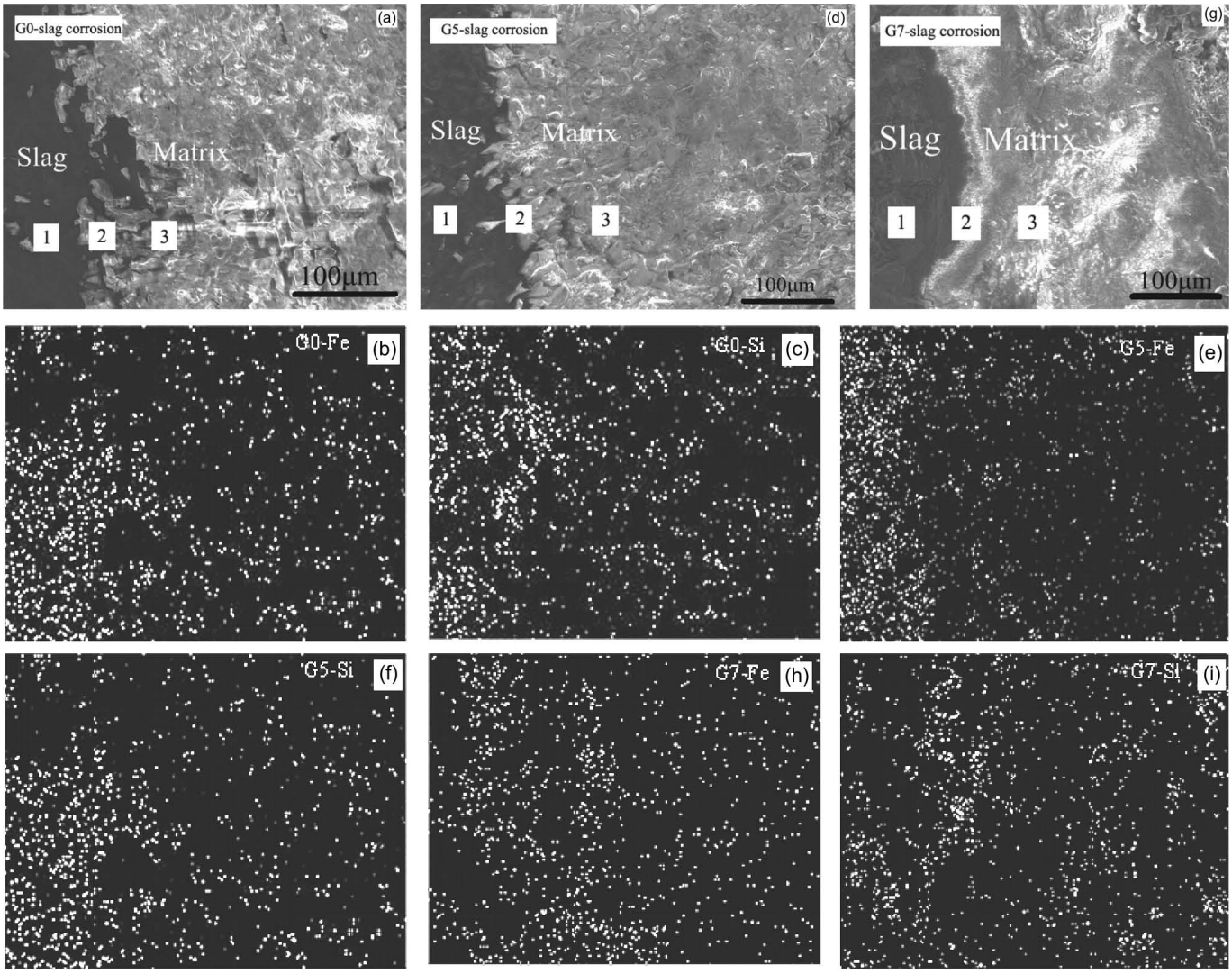

Fig. 7: SEM image of the erosion interface in G0 (a), G5 (d), G7 (g) after slag corrosion and EDS images of elements of the slag corrosion interface in G0, G5 and G7.

Table 4: The relative mass fraction (wt%) of Fe_2O_3 and SiO_2 at different penetration depth in G0 ~ G7 samples after slag corrosion (2 as demarcation point).

Project	G0		G4		G5		G6		G7	
	Fe_2O_3	SiO_2	Fe_2O_3	SiO_2	Fe_2O_3	SiO_2	Fe_2O_3	SiO_2	Fe_2O_3	SiO_2
Point 1 (-0.07mm)	53.29 ± 0.04	2.78 ± 0.06	58.62 ± 0.03	3.12 ± 0.03	50.69 ± 0.02	2.59 ± 0.03	54.62 ± 0.02	3.05 ± 0.02	55.60 ± 0.03	2.89 ± 0.04
Point 2 (0mm)	45.04 ± 0.03	0.93 ± 0.06	44.21 ± 0.03	0.89 ± 0.05	40.85 ± 0.04	0.87 ± 0.03	43.05 ± 0.07	0.92 ± 0.03	42.23 ± 0.06	0.95 ± 0.02
Point 3 (+0.07mm)	12.56 ± 0.04	0.29 ± 0.06	10.13 ± 0.02	0.27 ± 0.03	6.61 ± 0.03	0.24 ± 0.05	9.15 ± 0.03	0.31 ± 0.02	10.01 ± 0.06	0.27 ± 0.04

Table 5: The relative mass fraction (wt%) of Cu after crude copper corrosion of G0~G7.

Project	Cu mass fraction/%				
G0	G4	G5	G6	G7	
Point 1 (-0.07mm)	41.39 ± 0.05	46.24 ± 0.04	45.39 ± 0.04	44.25 ± 0.04	43.71 ± 0.03
Point 2 (0mm)	20.60 ± 0.02	18.31 ± 0.03	8.46 ± 0.05	16.20 ± 0.02	18.13 ± 0.03
Point 3 (+0.07mm)	5.33 ± 0.02	4.98 ± 0.02	3.52 ± 0.02	4.57 ± 0.03	4.91 ± 0.03

(5) The mechanism of slag/copper resistance

In general, there are four potential methods of slag penetration into a refractory, such as open porosity, grain boundary, network formed by impurity liquid and the lattice. Slag penetration into the refractory through the lattice and grain boundary is generally slow, which could be negligible in the refractory. The liquid phase formed by impurity was not observed in the SEM photos. Therefore, the open porosity was considered as the main channel in the slag/copper corrosion of the refractory. Some researchers believe that slag penetration depth in the refractory depends upon the following equation [18]:

$$L = (\sigma r t \cos\theta / 2\eta)^{1/2} \quad (1)$$

Where L is the slag penetration depth of refractory materials, σ is the surface tension of the slag, t is the penetration time, r is the porosity radius of the refractory materials, θ is the contact angle between the slag and refractory materials, η is the slag viscosity.

According to the equation, lower open porosity and higher slag viscosity could decrease penetration depth [5]. G5 had a low porosity (13 wt%), reducing the penetration channel of the slag in the brick. In addition, FeO in the slag and crude copper was able to dissolve into lattice vacancies in $MgAl_2O_4$ alumina-rich spinel solid solution and formed $Mg(Fe, Al)O_4$ (Fig. 6 (a)), which led to the increase in slag viscosity and the slag melting point, thus hindering the fast penetration of molten slag [15]. Therefore, sample G5 exhibited better corrosion resistance than the other samples.

(6) Microstructure changes in the ACR crucible after copper corrosion

The microstructures at the copper/matrix interface of the ACR crucible corroded by copper with slag are presented in Fig. 8. The copper with slag layer and the matrix were observed in all samples with a clear interface. The relative content of Cu elements at different points in slag (1), interface (2) and matrix (3) are given in Table 5. It can be seen that the content of Cu elements at point 2 and 3 in the refractory G5 was lower than in other samples. This can be attributed to the low porosity of G5, the Cu_2O mainly penetrated along the grain boundaries and open porosity into the refractory. The continuous black island structure and some big pores are also observed (point 4) in Fig. 8 (a) and (c), while the island structure area in sample G5 was less than in other samples. The EDS analysis shows that the black island structure in G0 was mainly composed of Al, Cr, Cu, Fe and O elements (Fig. 8(d)), indicating a large amount of copper with slag liquid had infiltrated into the internal matrix of G0 and G7.

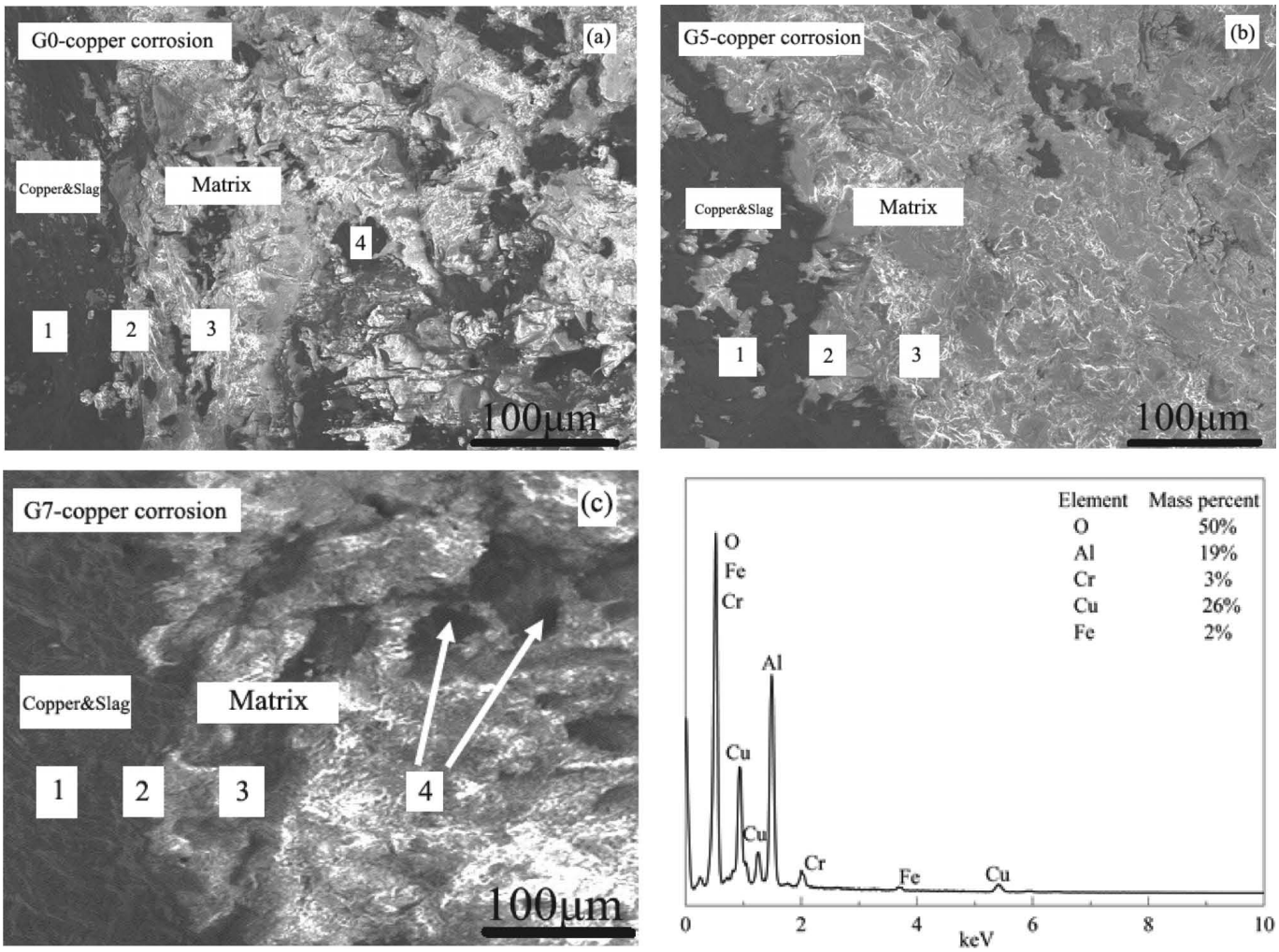

Fig. 8: SEM of G0 (a), G5 (b), G7 (c) after crude copper corrosion and EDS of point 4 (c) after crude copper corrosion.

IV. Conclusions

Using ACS of different grades (5 ~ 3 mm, 3 ~ 1 mm, 1 ~ 0 mm, 0.088 mm and 0.045 mm) as raw material, with added $MgAl_2O_4$ micron-grade powders, ACR was obtained after sintering at 1500 °C for 22 h.

(1) With 5 wt% $MgAl_2O_4$ spinel, ACR could be sintered to a bulk density of 3.25 g·cm^{-3} and apparent porosity of 13 %.

(2) $MgAl_2O_4$ spinel as an additive improved the slag corrosion and penetration resistance of ACR by 33.3 % and crude copper corrosion and penetration resistance by 42.8 % owing to the lower porosity and generation of $Mg(Fe, Al)O_4$.

Acknowledgment

The work is supported by Industry-Study-Research Projects of the Science and Technology Commission of Baoshan District, Shanghai, China (bkw2014134), National Science Foundation of China (Nos. 51272154), the Shanghai natural science fund (14ZR1416400), the production project in Guangdong province (2013B090600025), Technology Bureau of Panzhihua for Social Promotion Project (2015CY-S-1), the produce-learn-research projects from Pangang company (PGYCKJ006 – 2015). The authors also wish to express their thanks to the Instrumental Analysis and Research Center of Shanghai University for the experimental assistance with the TEM, XRD and SEM.

References

1 Nath, M., Sen, S., Banerjee, K., Ghosh, A., Tripathi, H.S.: Densification behavior and properties of alumina-chrome ceramics: effect of TiO_2, *Ceram. Int.*, **39**, 227 – 232, (2013).

2 Nath, M., Dana, K., Gupta, S., Tripathi, H.S.: Hot corrosion behavior of slip-cast alumina-chrome refractory crucible against molten glass, *Mater. Corros.*, **65**, 742 – 747, (2014).

3 Cooper, S.A., Nicholson, P.S.: Influence of glass redox conditions on the corrosion of fusion-cast chrome-alumina refractories, *Am. Ceram. Soc. Bull.*, **59**, 715 – 717, (1980).

4 Edme, E., Poirier, J., Bouchetou, M.L., Arnouil, J.P.: Improvement of chrome-alumina refractory lining in vitrification units for the treatment of fly ashes and asbestos hazardous wastes. In: *InterCeram*: International Ceramic Review. Expert Fachmedien GmbH, Düsseldorf, Germany, 2011.

5 Hirata, T., Morimoto, T., Ohta, S., Uchida, N.: Improvement of the corrosion resistance of alumina-chrome ceramic materials in molten slag, *J. Eur. Ceram. Soc.*, **23**, 2089 – 2096, (2003).

6 Popov, O.N., Frolova, V.P., Kirilenko, V.I., Tokarev, V.D.: Chrome-corundum refractory in the packing for a glass furnace regenerator, *Glass. Ceram.*, **48**, 13 – 17, (1991).

7 Cook, R.S., Fausey, W.H.: Casting of a chrome-alumina monolithic lining for melting insulation fiberglass in a cold-top electric melter, M. G. Wheeler, D. L. Smathers and D. G. Patel, *Ceram. Eng. Sci. Proc.*, **24**, 253 – 270, (2003).

[8] Chen, D., Huang, A., Gu, H., Zhang, M., Zhang, Z.: Corrosion of Al_2O_3-Cr_2O_3 refractory lining for high-temperature solid waste incinerator, *Ceram. Int.*, **41**, 14748 – 14753, (2015).

[9] Bonar, J.A., Kennedy, C.R., Swaroop, R.B.: Coal-ash slag attack and corrosion of refractories, *Am. Ceram. Soc. Bull.*, 59, 473 – 478, (1980).

[10] Mafliet, A., Lotfian, S, Scheunis, L., Petkov, V., Pandelaers, L., Jones, P. T., Blanpain, B.: Degradation mechanisms and use of refractory linings in copper production processes: A critical review, *J. Eur. Ceram. Soc.,* 34, 849 – 876, (2014).

[11] Petkov, V., Jones, P.T., Boydens, E., Blanpain, B., Wollants, P.: Chemical corrosion mechanisms of magnesia-chromite and chrome-free refractory bricks by copper metal and anode slag, *J. Eur. Ceram. Soc.*, **27**, 2433 – 2444, (2007).

[12] Tripathi, H.S., Das, S.K., Ghosh, A.: Effect of compositional variation on the synthesis of magnesite-chrome composite refractory, *Ceram. Int.*, **30**, 911 – 915, (2004).

[13] Hirata, T., Morimoto, T., Morimoto, A., Uchida, N.: Corrosion resistance of alumina-chromia ceramic materials against molten slag, *Mater. Trans.*, **43**, 2561 – 2567, (2002).

[14] Gehre, P., Aneziris, C.G., Berek, H., Parr, C., Reinmoller, M.: Corrosion of magnesium aluminate spinel-rich refractories by sulphur-containing slag, *J. Eur. Ceram. Soc.*, **35**, 1613 – 1620, (2015).

[15] Pilli, V., Sarkar, R.: Effect of spinel content on the properties of Al_2O_3-SiC-C based trough castable, *Ceram. Int.*, 42, 2969 – 2982, (2016).

[16] Braulio, M.A.L., Rigaud, M., Buhr, A., Parr, C., Pandolfelli, V. C.: Spinel-containing alumina-based refractory castables, *Ceram. Int.*, **37**, 1705 – 1724, (2011).

[17] Wang, W.X., Xing, J.D., Jin, Z.X.: Chemical reaction of Cu_2O-al system in preparation of Al_2O_3/Cu composite, *Rare. Metal. Mater. Eng.*, **36**, 679 – 682, (2007).

[18] Yin, Y., Liang, Y., Ge, S., Ge, Z., Nie, J., Lu, J.: Pore evolution and its effect on slag resistance of Al_2O_3-SiC-C castables, *J. Ceram. Soc. Jpn.*, **121**, 873 – 879, (2013).